IEEE Access
Multidisciplinary | Rapid Review | Open Access Journal

Date of publication xxxx 00, 0000, date of current version xxxx 00, 0000.

Digital Object Identifier 10.1109/ACCESS.2022.Doi Number

Novel Design Method for Millimeter-wave Gap Waveguide Low-Pass Filters Using Advanced Manufacturing Techniques

D. Santiago[1], M.A.G. Laso[1], T. Lopetegi[1], and I. Arregui[1]

[1]Institute of Smart Cities (ISC), Department of Electrical, Electronic and Communications Engineering, Public University of Navarre (UPNA)

Corresponding author: D. Santiago (e-mail: david.santiago@unavarra.es).

This work was funded by the Spanish Ministerio de Ciencia e Innovación –Agencia Estatal de Investigación (MCIN/AEI/ 10.13039/501100011033) under Project PID2020-112545RB-C53.

ABSTRACT In this paper, a groove gap waveguide (GGW) low-pass filter is proposed for the first time. Gap waveguide technology represents an interesting alternative as a low-loss, cost-effective, high-performance transmission line and packaging solution for microwave and millimeter-wave systems. This technology may exhibit a frequency behavior similar to rectangular waveguide but with some advantages such as the no need of electrical contact between the upper and lower plates of the GGW, making it an attractive alternative in the design of satellite devices at high frequencies. However, all the previous literature focused on band-pass filters, while design methods for GGW low-pass filters have not been reported. Furthermore, in this paper a new manufacturing approach is proposed and its performance has been compared with traditional methods such as Computer Numerical Control (CNC) milling. The new approach relies on the Selective Laser Melting (SLM)-3D printing of the filter followed by a post-processing step, in which it is partially mechanized using CNC milling to improve the surface finish. Measurements of the manufactured prototypes are also included to compare both techniques at millimeter-waves, showing the advantages of the new fabrication method and the excellent agreement with the simulations.

INDEX TERMS Groove gap waveguide, low-pass filter, selective laser melting 3D-printing.

I. INTRODUCTION

The gap waveguide technology was introduced in [1], [2] as an alternative to conventional waveguides for high frequencies. Specifically, the groove gap waveguide (GGW) technology is based on two metal parallel plates, where one of them exhibits a pin bed. This pin bed usually consists of multiple square metal pins, as we can see in Fig.1. The pin structure introduces a high impedance condition at the plane above the pins. Thus, by placing the other (flat) metal plate at a gap distance < $\lambda/4$ from the top of the pins, the propagation in the pin region is forbidden over a certain frequency range defined by the periodicity of the pin structure, provided also that the height of the pins is approximately $h = \lambda/4$ to create the high impedance condition. Comprehensive studies about the most important parameters of the GGW have been presented in [3]-[6]. The main advantage of the GGW is that it allows the wave propagation along the channel defined by W and L in Fig.1, with a similar performance as a rectangular waveguide of width W and height L, as explained in [7], [8]. Using this technology, several devices have been reported, for instance antennas [9]-[11] or bandpass filters based on coupled resonators [12]-[14]. However, no design technique is available in the literature for low-pass filters, which benefit from the inherent advantages of frequency responses not based on resonances.

Currently, rectangular waveguide filters are key components in many practical applications, with special presence in the fields of radar and communications [15], [16]. In [17], Cohn proposed the classical corrugated low-pass filter and the design technique was described in the well-known book written by Matthaei, Young, and Jones [18]. The method consists of a cascade of rectangular waveguide sections with the same width but different height. Unfortunately, while GGW technology seems suitable for changes in the filter width, there is no easy way to implement changes in the filter height as there are restrictions in the height of the pins and the gap distance in order to keep the nature of the technology itself, as

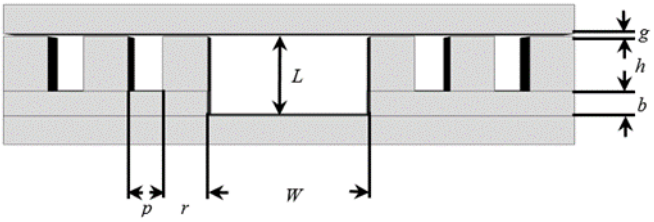

FIGURE 1. Section of the groove gap waveguide structure.

explained before. Hence, GGW technology cannot be used straightforwardly for corrugated low-pass filters and, therefore, a different GGW topology is introduced in this paper to achieve the low-pass frequency response.

Once a low-pass filter is designed in the new GGW topology, its manufacturing is studied considering that we aim for high (millimeter-wave) frequencies. Complex manufacturing methods can be used to fabricate millimeter-wave filters and, in [19], a description of some of these emerging techniques is presented. However, CNC milling is still the most widespread method for fabricating metal waveguide components due to its simplicity and good performance at lower frequencies. On the other hand, Additive Manufacturing (AM) has recently received much attention as a key technology for the integration of millimeter-wave systems and it seems especially suitable for the fabrication of GGW devices, since it allows the implementation of a large number of pins (if required) without increasing (unlike CNC milling) the time or cost of the process as explained in [20], where a comparison between several manufacturing methods is presented. Among the several AM processes available in the market, the so-called stereolithographic (SLA) 3D-printing method [21], [22], is rapidly evolving, being a promising alternative to CNC milling in some applications and benefiting from the inherent general advantages of 3D-printing for RF components. It can precisely print the parts in a polymer, which has to be later on plated. Plating a GGW is not complex, as it consists of open surfaces easily accessible for the silver or gold, for instance, to deposit. However, in space applications this approach poses some important problems, such as the different coefficient of thermal expansion of both the polymer and the metal. A more promising approach for space is 3D-printing by Selective Laser Melting (SLM) [23], [24], where the system is directly fabricated in metal (aluminum, for instance). Unlike SLA, SLM has the advantage of not requiring a subsequent postprocessing (plating). However, although its disadvantages are rapidly improving, SLM still has lower printing precisions and more surface roughness, which are of particular importance for millimeter-wave filters. In order to cope with these disadvantages while we benefit from the advantages of SLM, a postprocessing step consisting in mechanizing only part of the 3D-printed filter

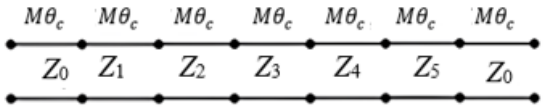

FIGURE 2. 5th-order transmission line filter prototype.

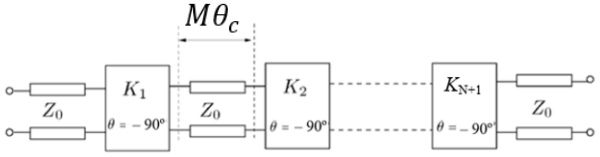

FIGURE 3. Equivalent circuit of a low-pass filter of order *N* based on impedance inverters connected with transmission-line sections.

is explained in this work.

In summary, in this paper the first GGW low-pass filter is proposed. To this end, the new GGW filter topology will be introduced in Section II along with the low-pass design procedure, where the filter will consist of transmission-line sections and impedance inverters. Finally, a combined 3D-printing and milling fabrication method will be explained in Section III, benefiting from the advantages of SLM and fighting against its disadvantages with a mechanization postprocessing of part of the 3D-printed filter. A design example will be given in Section IV to show the good electrical performance of our approach and some conclusions will close this work.

II. DESIGN METHOD

A classical corrugated waveguide low-pass filter consists of a cascade of transmission-line sections, each of them characterized by its impedance, Z_i, as depicted in Fig. 2, where a stepped impedance network is shown following [16]. In order to implement it in rectangular waveguide, this approach would lead to sections where the height changes. As we have previously said, implementing changes in height is not straightforward in GGW, since the pin height and the gap are critical parameters in this technology and their change affects the electrical behavior of the pin bed. In rectangular waveguide technology, an interesting alternative was presented in [25] for the implementation of high-power low-pass filters consisting of transmission-line sections connected through impedance inverters, whose values change to keep the same characteristic impedance in all the transmission-line sections. The values of the impedance inverters are obtained by full-wave simulation tools, and they allow the implementation of low-pass filters in rectangular waveguide through obstacles that extend completely along the broad direction of the waveguide. In Fig. 3, we can see an equivalent circuit showing the impedance inverters, K_i, connected to transmission-line sections of equal impedance, Z_0. In order to allow the implementation of low-pass devices for millimeter-wave frequencies, this approach is extended to

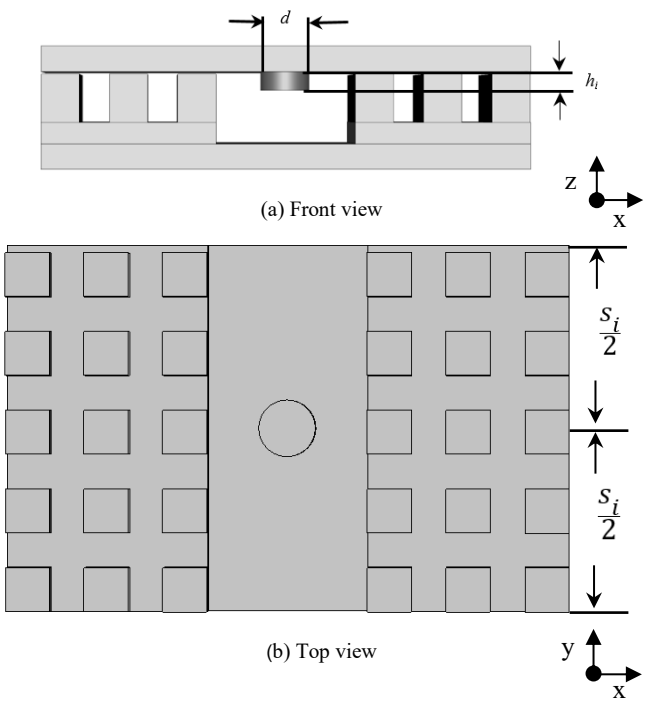

FIGURE 4. Post inside a groove gap waveguide section employed as an impedance inverter.

overcome the limitation of using transmission lines with electrical length just equal to θ_c, as required in [25] and [26]. As a matter of fact, the use of longer transmission lines, represented as $M\theta_c$ (where $M \geq 1$ is an integer number) in Figs. 2 and 3, will have a similar effect than the use of higher-order modes when designing bandpass filters, as detailed in [27] and [28]. The particular case of $M = 1$ leads to the techniques presented in [25] and [26], while increasing M provides benefits for millimeter-wave applications. Indeed, in addition to the robustness against manufacturing errors needed for high frequency components, the larger separation between the inverters as M increases leads to a more accurate design approach since the possible interaction of the adjacent inverters (not considered in the design method) is reduced as the distance between them is larger.

The low-pass filter synthesis procedure begins by fixing the order of the filter, N, which determines the number of transmission-line sections, the in-band return loss level, RL, the maximum frequency of the passband, f_c, and the maximum rejection frequency, f_0. With these values, we can calculate the $M\theta_c$ value as:

$$M\theta_c = 90 \cdot M \cdot \frac{\lambda_{g,f_0}}{\lambda_{g,f_c}} \quad (1)$$

where λ_{g,f_0} and λ_{g,f_c} are the guided wavelength corresponding to f_0 and f_c, respectively. Therefore, the spurious-free band can be controlled by modifying this parameter. Once we have obtained the impedances of the transmission-line sections, we

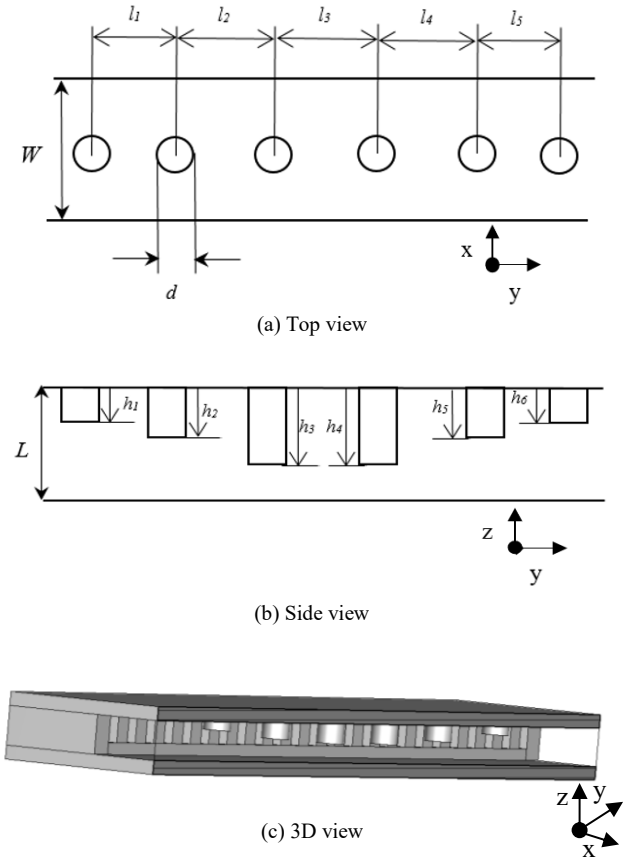

FIGURE 5. Low-pass filter based on circular posts (filter order N = 5).

can determine the values of the impedance inverters following the methodology outlined in [25]. However, in the case of GGW technology, we need to implement a feasible topology that, unlike [25], differs from using obstacles of different geometries extending along the entire broad direction of the waveguide. As mentioned before, each impedance inverter is connected to two transmission lines of equal characteristic impedance, Z_0, and electrical length $M\theta_c$. The impedance inverter can be physically implemented in GGW by using a post of diameter d and height h_i, see Fig. 4. The post is connected to two GGW sections of length $s_i/2$, which is half of the separation between the surrounding impedance inverters in Fig. 3 (i.e., $M\theta_c/2$). Moreover, as can be also seen in Fig. 4, these posts can be placed in the top plate, so that the posts and the pin bed in the bottom plate do not condition each other during the manufacturing process and can be easily and independently fabricated.

The characterization of the circular posts as impedance inverters can be accomplished by using an electromagnetic simulator such as CST MWS. This will allow us to obtain their final physical dimensions. The magnitude of the scattering parameter is primarily influenced by the post height, while the phase is mainly affected by the position of the port reference

planes. In the equivalent circuit depicted in Fig. 3, the values of the normalized inverters K_i/Z_0 can be related to the transmission parameter of the structure, as described in [25], through:

$$|S_{21}| = \frac{2}{\frac{K_i}{Z_0}+\frac{1}{\frac{K_i}{Z_0}}} \qquad i = 1, 2, \ldots, N+1 \tag{2}$$

being $|S_{21}|$ the transmission parameter magnitude. Once we have calculated the value of $|S_{21}|$, the height of the post, h_i, is varied until this is obtained at the maximum frequency of the passband, f_c. Note that this process can be applied placing the ports at an arbitrary distance, since the value of $|S_{21}|$ remains unaffected. Once the appropriate height, h_i, is determined, the next step of the design procedure is to calculate s_i, while considering the loading effect of the post. The phase of the transmission parameter can be represented as a function of the distance from the auxiliary input/output ports to the post (s_i/2). On the other hand, the phase of the transmission parameter is calculated using $M\theta_c$ from (1) as follows:

$$\Phi(S_{21}) = -M\theta_c - 90° \tag{3}$$

where the phase shift introduced by a capacitive impedance inverter is –90º and $M\theta_c$ denotes the electrical length of the transmission lines connecting the inverters. If an inductive impedance inverter is used, the phase shift would be calculated by adding +90° instead of -90°. Again, s_i is varied until the calculated value of $\Phi(S_{21})$ is obtained at f_c. The final separations between the posts (l_i) in Fig.5 will be calculated as:

$$l_i = \frac{s_i}{2} + \frac{s_{i+1}}{2} \qquad i = 1, 2, \ldots, N \tag{4}$$

The same process is repeated to adjust all the heights of all the posts in the structure, h_i, as well as their s_i, thus implementing all the impedance inverters and transmission-line sections. In the last step, the final topology of the filter is reconstructed by connecting all the transmission-line sections with their corresponding posts, resulting in a structure resembling that in Fig. 5(c). It is worth noting that, in this final step, the coupling or interactions between the different posts are not taken into account, so a final optimization may be necessary to achieve the desired response.

III. ADVANCED MANUFACTURING METHOD

Nowadays, Additive Manufacturing (AM) is one of the drivers of change in the new Industry 4.0 paradigm. AM applied to space platforms appeared some years ago as an enabling technology for satellite RF/microwave devices, Internet of Space (IoS), and space-based Internet of Things (IoT) applications [29]. In the context of RF/microwaves, some of the most promising AM techniques are the fused deposition modeling (FDM) of polymers, polymer and ceramic stereo-lithography (SLA), and selective laser melting of metals (SLM). SLM is very attractive in the sense that the printed part is already metallic (aluminum, for instance) [30], [31]. On the other hand, polymer-based AM produces lighter components and very accurate dimensions, while ceramic-based parts benefit from low loss/high permittivity dielectric materials. However, plating and metallizing dielectric-based parts, including their inner waveguides, pose significant challenges. Although alternatives have been proposed based on sputtering or electroless plating, they are not simple. Despite of its advantages, the surface roughness achieved with SLM usually affects the behavior of the prototype, as [32] and [33] explained in detail. This roughness is especially detrimental when operating at high frequencies, being not possible to obtain components with a similar performance than the ones fabricated by milling, as commented in [34]. Therefore, SLM is typically avoided when implementing millimeter-wave devices, especially filters, which are very demanding in terms of final manufacturing quality. However, in our case of low-pass GGW filters, we could easily machine the GGW channel and the top-plate posts, as a postprocessing step once the filter has been 3D-printed, so that roughness is improved in the surfaces that directly interact with the propagating wave. Using post-processing procedures after 3D-printing is something usual and they typically range from metallization to thermal treatment [35]-[37], which are techniques that unfortunately can significantly worsen the manufacturing accuracy. In our case, we propose a manufacturing method that combines SLM 3D-printing with a straightforward CNC milling step in the postprocessing phase, taking benefit of all the advantages of SLM and avoiding its disadvantages (roughness mainly). Moreover, the design technique contributes to the overall filter robustness in the

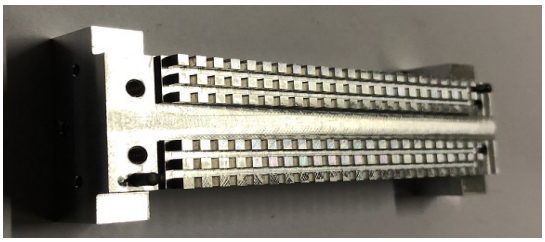

(a) CNC-milled straight GGW line

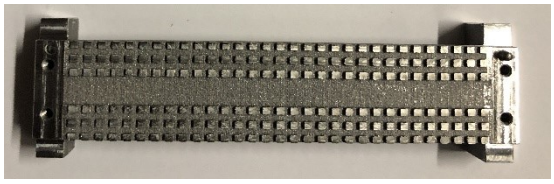

(b) SLM-3D printed straight GGW line

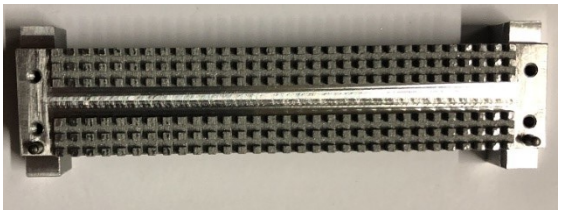

(c) Straight GGW line manufactured by the combined (3D-printing plus milling) method proposed in this paper

FIGURE 6. GGW prototypes: straight waveguides.

millimeter-wave range as explained before. As typically done, the external flange is also machined to ensure a perfect match with the measuring equipment. Unlike the GGW channel and the top-plate posts, machining the GGW pin bed (which would be very costly and time consuming) is not needed as it does not affect the overall device operation.

In order to show the potential of this combined SLM plus CNC milling manufacturing process for millimeter-wave GGW devices, several straight GGW lines will be designed, fabricated, and compared. In particular, we will consider these three manufacturing methods: (a) conventional CNC milling, (b) SLM 3D-printing, and (c) SLM 3D-printing plus CNC milling as a postprocessing step. In all three cases, the flanges will be machined and the GGW employs the same dimensions (see Fig.1): $W = 5.69$ mm, $L = 2.845$ mm, $g = 0.1$ mm, $h = 1.9$ mm, $r = 1.56$ mm, and $p = 1.23$ mm. With the aim of keeping the dimensions of the WR22 standard ports ($W = 5.69$ mm, $L = 2.845$ mm), a pedestal of height $b = 0.845$ mm is added. The prototypes, which have a length equal to 100 mm, are shown in Fig. 6. A simple visual inspection reveals that the waveguide roughness is easily perceptible in the case of the SLM 3D-printed (without any machining postprocessing) device, Fig. 6(b), compared to the other 2 prototypes: Fig. 6(a) is a wholly machined GGW line, while Fig. 6(c) is a 3D-printed GGW line where the GGW channel is machined after 3D-printing. In terms of the GGW pin bed, Fig. 6(b) and Fig. 6(c) look of course very similar. The behavior of the device is not affected by the roughness in the pin bed, as explained before and, hence, no mechanization is needed in this region.

In order to evaluate the frequency behavior of the structures manufactured by the three approaches, the effective conductivity obtained from the S_{21} and from the loss L-parameter, defined as in [38], are compared. In addition to the S_{21}, which is the typical parameter considered to evaluate the insertion loss of a component, L is also shown here to involve the S_{11} parameter in the analysis and unmask artifacts that may appear in the S_{21} due to manufacturing or assembly. Specifically, for the 2-port devices considered in this analysis, L is estimated as [38]:

$$L = -10\log(|S_{11}|^2 + |S_{21}|^2) \quad (5)$$

The expression in (5) simply represents the conservation of energy in the component. The three GGWs have been measured under the same environment in the same test campaign in order to avoid imbalances in the measurement equipment and calibration. A comparison of the three measurements is shown in Fig. 7: L is given in Fig. 7(a) and the transmission parameter ($|S_{21}|$) in Fig. 7(b).

All three straight GGW lines have WR22 ports and, hence, comparisons are made over the 33-50 GHz frequency range. For comparison purposes, we have also included the CST MWS simulations considering PEC (black line), as well as

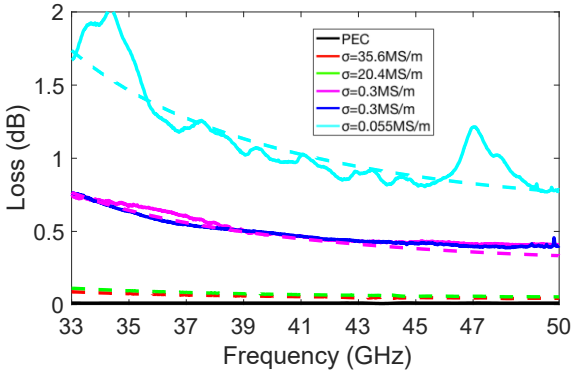

(a) Loss L for the straight GGW lines

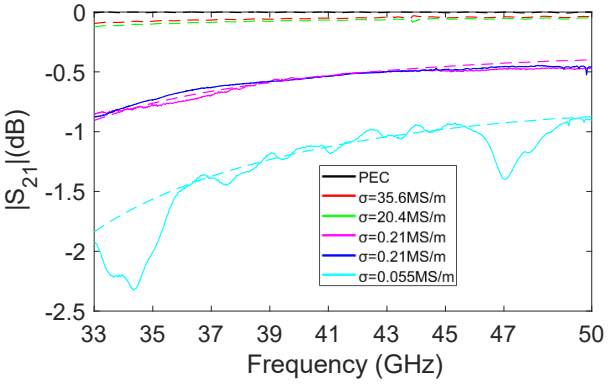

(b) $|S_{21}|$ for the straight GGW lines

FIGURE 7. Comparison of the conductivity achieved between the GGW using PEC (black line), aluminum (red line), $AlSi_{10}Mg$ (green line), and the measured results of the manufactured prototypes with CNC milling (magenta line), the advanced manufactured technique (blue line), and SLM 3D-printing (cyan line). Simulation results in dashed line and measurement results in solid line.

aluminum (red line), which is the material used for the CNC milled GGW line with an ideal conductivity of 35.6 MS/m, and $AlSi_{10}Mg$ (green line), which is the material employed for SLM 3D-printing with an ideal conductivity of 20.4 MS/m. In the same figure, we show the measurements of the CNC-milled prototype (magenta line) and of the 3D-printed prototype after the milling postprocessing (blue line). As can be seen in Fig. 7(a), both measurements show an effective conductivity which corresponds with a value equal to 0.3 MS/m. This effective conductivity considers the background material conductivity as well as effects such as the roughness of the walls. The measured effective conductivity for the SLM 3D-printed GGW line without any machining postprocessing is 0.055 MS/m (cyan line), i.e. 6 times lower than using the postprocessing. Moreover, L shows also a greater variation in the WR22 bandwidth for the case of not using postprocessing due to dimension inaccuracies in the fabrication.

These results agree with the $|S_{21}|$ results shown in Fig. 7(b), where the CNC-milled prototype and the 3D-printed prototype after postprocessing reach again the same value for the

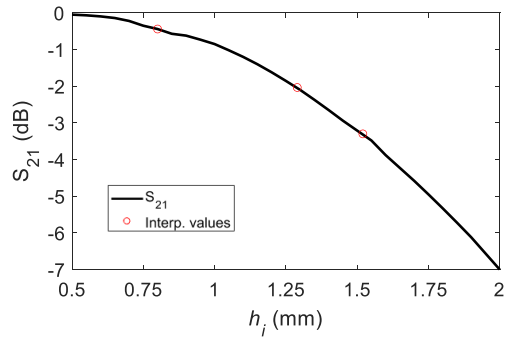

FIGURE 8. Magnitude of the transmission parameter ($|S_{21}|$) of the structure in Fig. 4 as a function of the height of the post. Circles show the interpolated values required for the design of the filter with $N = 5$.

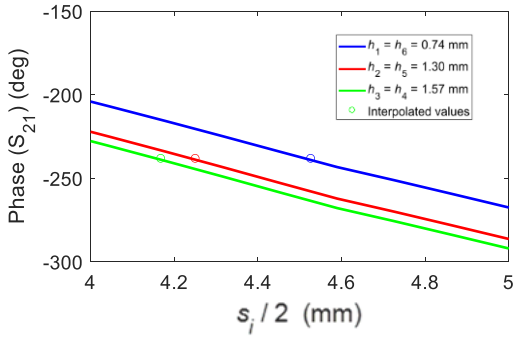

FIGURE 9. Phase of the transmission parameter ($\Phi(S_{21})$) of the structure in Fig. 4, as a function of the GGW section half-length ($s_i/2$). Circles show the interpolated values required for the design of the filter with $N = 5$.

effective conductivity, 0.21 MS/m, quite near to the value estimated with *L*. Something similar occurs with the SLM 3D-printed GGW line without any machining postprocessing. As expected, the SLM 3D-printed device with the machining postprocessing has, in the region where the wave propagates, similar physical characteristics as the wholly milled device and, in particular, the surface roughness is also similar. The differences would be mainly due to the conductivity of the background material. At the same time, these results somehow contradict [6], where SLM-3D printing was discarded as an alternative to fabricate gap waveguide devices due to the roughness of the device manufactured with this method. From these measurements, we can conclude that only a simple machining of the critical parts would be necessary to combine all the advantages of 3D printing, such as the quick and inexpensive fabrications of intricate features like the GGW pin bed, with the electrical performance achieved with CNC milling.

In the next Section, we will make use of this new fabrication approach to design and manufacture several low-pass GGW filters. Again, comparisons will be done between wholly milled parts and parts fabricated using the combined 3D-printing/milling approach.

TABLE 1 Physical and electrical parameters for the filter with $N = 3$ and $M\theta_c = 148°$

GGW Section	Z_i (1: N)	l_i (mm) (1: N)	K_i / Z_o (1: $N+1$)	$\|S_{21}\|$ (dB)	h_i (mm) (1: $N+1$)
1	0.61	9.24	$K_1/Z_o = 0.78$	-0.28	0.66
			$K_2/Z_o = 0.61$	-1.02	1.09
2	1.61	8.91			
			$K_3/Z_o = 0.61$	-1.02	1.09
3	0.61	9.24			
			$K_4/Z_o = 0.78$	-0.28	0.66

TABLE 2 Physical and electrical parameters for the filter with $N = 5$ and $M\theta_c = 148°$

GGW Section	Z_i (1: N)	l_i (mm) (1: N)	K_i / Z_o (1: $N+1$)	$\|S_{21}\|$ (dB)	h_i (mm) (1: $N+1$)
1	0.53	9.04	$K_1/Z_o = 0.73$	-0.44	0.74
			$K_2/Z_o = 0.49$	-2.03	1.30
2	2.18	8.56			
			$K_3/Z_o = 0.39$	-3.29	1.57
3	0.34	8.44			
			$K_4/Z_o = 0.39$	-3.29	1.57
4	2.18	8.56			
			$K_5/Z_o = 0.49$	-2.03	1.30
5	0.53	9.04			
			$K_6/Z_o = 0.73$	-0.44	0.74

TABLE 3 Physical and electrical parameters for the filter with $N = 7$ and $M\theta_c = 148°$

GGW Section	Z_i (1: N)	l_i (mm) (1: N)	K_i / Z_o (1: $N+1$)	$\|S_{21}\|$ (dB)	h_i (mm) (1: $N+1$)
1	0.51	9.16	$K_1/Z_o = 0.71$	-0.49	0.73
			$K_2/Z_o = 0.47$	-2.31	1.23
2	2.33	8.76			
			$K_3/Z_o = 0.36$	-3.84	1.46
3	0.31	8.66			
			$K_4/Z_o = 0.33$	-4.39	1.62
4	2.73	8.65			
			$K_5/Z_o = 0.33$	-4.39	1.62
5	0.31	8.66			
			$K_6/Z_o = 0.36$	-3.84	1.46
6	2.33	8.76			
			$K_7/Z_o = 0.47$	-2.31	1.23
7	0.51	9.16			
			$K_8/Z_o = 0.71$	-0.49	0.73

IV. DESIGN EXAMPLE

The method described in Section II is used in this Section for the design of three low-pass GGW filters. First, we fix the return loss level, *RL*, and the order of the filter, *N*. In our case, we aim for a *RL* better than 20 dB and *N* consecutively takes the value of 3, 5, and 7 for each of the filters designed. $M\theta_c$ is calculated using (1), and for this we first define the maximum

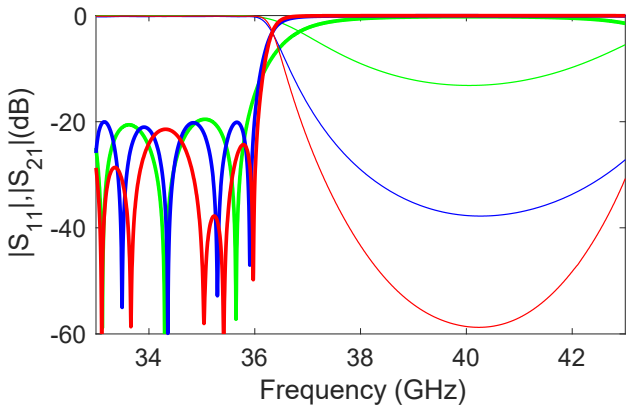

FIGURE 10. Comparison between the CST MWS simulated frequency response for the filter of order *N* = 3 (green line), *N* = 5 (blue line), and *N* = 7 (red line). $|S_{11}|$ in thick line and $|S_{21}|$ in thin line.

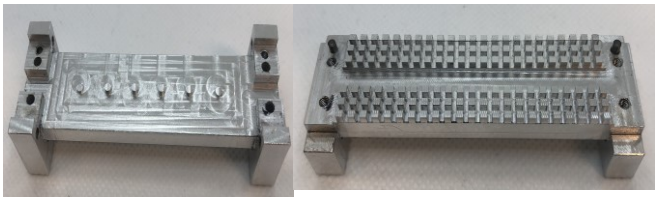

(a) CNC-milled devices

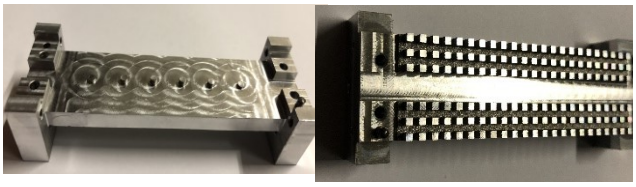

(b) Devices manufactured using the combined 3D-printing/milling approach used in this paper

FIGURE 11. Low-pass filters prototypes.

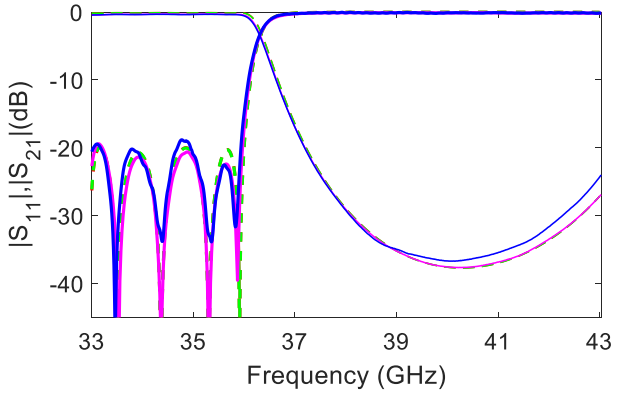

(a) S-Parameters

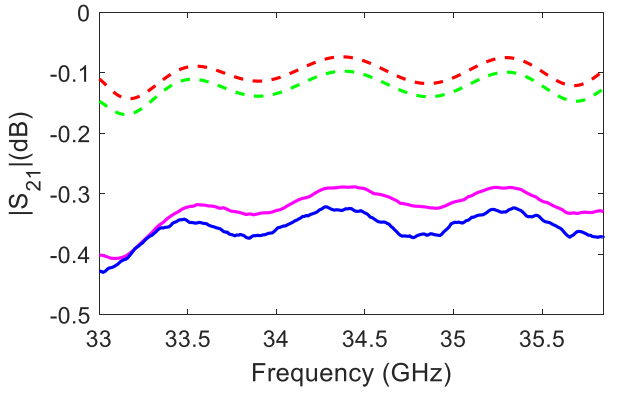

(b) Insertion loss

FIGURE 12. Comparison between the CST MWS simulated frequency responses (dashed lines) for the filter of order *N* = 5 using different materials: aluminum (red line) and $AlSi_{10}Mg$ (green line). Measured results (solid lines) for the prototypes manufactured by CNC milling (magenta line) and the combined manufacturing technique described in this work (blue line). $|S_{11}|$ in thick line and $|S_{21}|$ in thin line.

frequency of the passband, f_c = 36 GHz, and the maximum rejection frequency, f_0 = 40 GHz. In these conditions, and considering $M = 2$, the electrical length $M\theta_c$ is 148º. Next, we proceed to calculate the transmission line impedances, Z_i, and the impedance inverters. Following the design method, we can calculate the $|S_{21}|$ parameter using (2) for each impedance inverter. Additionally, we determine the phase shift of the transmission parameter using (1) and (3). The values of h_i are variated until the desired $|S_{21}|$ parameter is achieved (using a post diameter, $d = 2$ mm), followed by adjusting the values of s_i until the correct $\Phi(S_{21})$ is reached, as explained below. The separation between the posts l_i will be finally obtained using (4). The final values of the physical and electrical parameters will be summarized in Table I, Table II and Table III for a filter order N = 3, 5, and 7, respectively. In order to obtain the correct h_i, the structure shown in Fig. 4 (a) is analyzed taking different post heights. In Fig. 8, we show the $|S_{21}|$ parameter at the maximum frequency of the passband, f_c, for different post heights (from 0.5 to 2 mm). The circles represent the interpolated value of h_i required for the filter of order N = 5, using (2) to implement the needed impedance inverters. Furthermore, the phase of the transmission parameter ($\Phi(S_{21})$) is also computed for the structure of Fig.4 (b) at the maximum frequency of the passband, f_c, as a function of the reference ports positions, $s_i/2$. This is shown in Fig. 9, where the phase is displayed for different lengths $s_i/2$ (from 4 to 5 mm) and using different post heights for the filter of order N = 5 (the heights previously calculated by means of Fig. 8). Again, the interpolated values are indicated with circles in the graph. As we explained before, the interaction between each post has not been considered in the design method (which would be minimized as $M\theta_c$ increases), and an optimization has to be made after cascading all the elements. That is the reason of the deviation between the theoretical values and the final heights and lengths in Tables I, II, and III. In Fig. 10, we can see the simulated frequency response of the filter with N = 3, 5, and 7. The higher the filter order, the greater the rejection level (around 60 dB for N = 7). The RL is around

20 dB in all three cases. The final design for $N = 5$ has been fabricated and is shown in Fig. 11, where Fig. 11(a) depicts the final prototype manufactured by CNC milling and Fig. 11(b) is the 3D-printed filter followed by a machining postprocessing. In Fig. 12, we also show a comparison between the CST MWS simulations using aluminum with a conductivity of 35.6 MS/m and the $AlSi_{10}Mg$ alloy with a conductivity of 20.4 MS/m for the filter of $N = 5$. The former is used for the wholly milled prototype, while the latter is the material used for 3D-printing. In Fig. 12 we can also see the measurements of the fabricated low-pass filters obtained by means of a Keysight E8361C PNA. Moreover, the insertion loss parameter is also given in detail, see Fig. 12 (b). An excellent agreement is observed between simulations and measurements. We can also interpret these results as a confirmation of the fact that the machining postprocessing has eliminated the surface roughness of the SLM 3D-printing, and hence the 3D-printed device behaves electrically as the wholly milled prototype as long as the machining postprocessing is employed. Moreover, its cost and lead time is much less, making this combined fabrication method an excellent alternative for millimeter-wave filters using GGW technology.

V. CONCLUSION

A technique to design low-pass filters in GGW technology has been proposed for the first time in this paper using posts as impedance inverters in the top-plate. The filters are 3D-printed using SLM and similar electrical performance as a prototype manufactured by milling is achieved as long as the 3D-printed filter is subjected to a machining postprocessing of only the GGW channel and the top-plate posts. This combines the overall flexibility and cost effectiveness given by 3D printing with the good performance of wholly milled parts. Several straight GGW lines and filters of different orders were designed, manufactured, and compared considering different fabrication techniques, showing that our approach is a promising way to design lower-cost low-pass filters in the millimeter-wave frequency range with lower lead times too.

REFERENCES

[1] P.-S. Kildal, E. Alfonso, A. Valero-Nogueira, and E. Rajo-Iglesias, "Local metamaterial-based waveguides in gaps between parallel metal plates," *IEEE Antennas and Wireless Propagation Letters*, vol. 8, pp. 84–87, 2009.

[2] P.-S. Kildal, "Waveguides and transmission lines in gaps between parallel conducting surfaces," European Patent Application EP08159791.6, 2008.

[3] A. Berenguer, V. Fusco, D.E. Zelenchuk, D. Sánchez-Escuderos, M. Baquero-Escudero, and V.E. Boria-Esbert, "Propagation characteristics of groove gap waveguide below and above cutoff," *IEEE Transactions on Microwave Theory and Techniques*, vol. 64, no.1, pp. 27-36, 2016.

[4] E. Rajo-Iglesias, and P.-S. Kildal, "Numerical studies of bandwidth of parallel-plate cut-off realized by a bed of nails, corrugations and mushroom-type electromagnetic bandgap for use in gap waveguides," *IET Microwave, Antennas and Propagation*, vol. 5, no. 3, pp. 282–289, 2011.

[5] E. Rajo-Iglesias, M. Ferrando-Rocher, and A.U. Zaman, "Gap waveguide technology for millimeter-wave antenna systems," *IEEE Communications Magazine*, vol. 56, no. 7, pp. 14-20, 2018.

[6] F. Fan, J. Yang, V. Vassilev, and A.U. Zaman, "Bandwidth investigation on half-height pin in ridge gap waveguide," *IEEE Transactions on Microwave Theory and Techniques*, vol. 66, no. 1, pp. 100-108, 2018.

[7] E. Rajo-Iglesias, and P. Kildal, "Groove gap waveguide: A rectangular waveguide between contactless metal plates enabled by parallel-plate cut-off," *Proceedings of the Fourth European Conference on Antennas and Propagation*, Barcelona, Spain, pp. 1-4. 2010.

[8] L. Miao, Z.H. Yan, W. Liu, and Y.B. Zhong, "Study of the characteristic of gap waveguide and comparison with rectangular waveguide," *International Workshop on Microwave and Millimeter Wave Circuits and System Technology*, pp. 72-75, 2013.

[9] M. Vukomanovic, J. Vazquez-Roy, O. Quevedo-Teruel, E. Rajo-Iglesias, and Z. Sipus, "Gap waveguide leaky-wave antenna," *IEEE Transactions on Antennas and Propagation*, vol. 64, no. 5, pp. 2055-2060, 2016.

[10] A.U. Zaman, and P. Kildal, "Slot antenna in ridge gap waveguide technology," *6th European Conference on Antennas and Propagation* (EUCAP), pp. 3243-3244, 2012.

[11] A.U. Zaman, and P. Kildal, "Wide-band slot antenna arrays with single-layer corporate-feed network in ridge gap waveguide technology," *IEEE Transactions on Antennas and Propagation*, vol. 62, no. 6, pp. 2992-3001, 2014.

[12] E.A. Alós, A.U. Zaman, and P. Kildal, "Ka-band gap waveguide coupled-resonator filter for radio link diplexer application," *IEEE Transactions on Components, Packaging and Manufacturing Technology*, vol. 3, no. 5, pp. 870-879, 2013.

[13] A.U. Zaman, P. Kildal, and A. Kishk, "Narrow-band microwave filter using high-Q groove gap waveguide resonators with manufacturing flexibility and no sidewalls," *IEEE Transactions on Components, Packaging and Manufacturing Technology*, vol. 2, no. 11, pp. 1882-1889, 2012.

[14] B. Ahmadi, and A. Banai, "Direct coupled resonator filters realized by gap waveguide technology," *IEEE Transactions on Microwave Theory and Techniques*, vol. 63, no. 10, pp. 3445-3452, 2015.

[15] V.E. Boria, and B. Gimeno, "Waveguide filters for satellites," *IEEE Microwave Magazine*, vol. 8, no. 5, pp. 60–70, 2007.

[16] R.J. Cameron, C.M. Kudsia, and R.R. Mansour, Microwave Filters for Communication Systems: Fundamentals, Design and Applications. Hoboken, NJ, USA: Wiley, 2007.

[17] S.B. Cohn, "A theoretical and experimental study of a waveguide filter structure," Office Naval Res., Cruft Lab., Harvard University, Cambridge, Mass., Rep. 39, 1948.

[18] G.L. Matthaei, L. Young, and E.M.T. Jones, Microwave Filters, Impedance-Matching Networks, and Coupling Structures. Norwood: Artech House, 1980.

[19] R.V. Snyder, G. Macchiarella, S. Bastioli, and C. Tomassoni, "Emerging trends in techniques and technology as applied to filter design," *IEEE Journal of Microwaves*, vol. 1, no. 1, pp. 317-344, 2021.

[20] P. Sanchez-Olivares, M. Ferreras, E. Garcia-Marin, L. Polo-López, A. Tamayo-Domínguez, J. Córcoles, J.M. Férnandez-Gónzalez, J.L. Masa-Campos, J.R. Montejo-Garai, J.M. Rebollar, J.A. Ruiz-Cruz, M. Sierra-Castañer, M. Sierra-Pérez, M. Barba, J.L. Besada, and J. Grajal, " Manufacturing guidelines for w-band full-metal waveguide devices: Selecting the most appropriate technology" *IEEE Antennas and Propagation Magazine*, vol. 65, no. 2, pp. 48-62, 2022.

[21] B. Liu, X. Gong, and W.J. Chappell, "Applications of layer-by layer polymer stereolithography for three-dimensional high-frequency components," *IEEE Transactions on Microwave Theory and Techniques*, vol. 52, no. 11, pp. 2567–2575, 2004.

[22] C. Guo, X. Shang, J. Li, F. Zhang, M.J. Lancaster, and J. Xu, "A lightweight 3-D printed X-band bandpass filter based on spherical dual-mode resonators," *IEEE Microwave and Wireless Components Letters*, vol. 26, no. 8, pp. 568–570, 2016.

[23] X. Wen, X. Shang, Y. Yu, M. Shu, Q. Yang, S. Li, M.M. Attallah, H. Liu, and A. Zhang, "SLM printed waveguide dual-mode filters with

reduced sensitivity to fabrication imperfections," *IEEE Microwave and Wireless Components Letters*, vol. 31, no. 11, pp. 1195-1198, 2021.
[24] C. Tomassoni, O.A. Peverini, G. Venanzoni, G. Addamo, F. Paonessa, and G. Virone, "3D printing of microwave and millimeter-wave filters: Additive manufacturing technologies applied in the development of high-performance filters with novel topologies," *IEEE Microwave Magazine*, vol. 21, no. 6, pp. 24–45, 2020.
[25] P.V. Castejón, D.C. Serrano, F.D.Q. Pereira, J. Hinojosa, and A. Álvarez Melcón, "A novel low-pass filter based on rounded posts designed by an alternative full-wave analysis technique," *IEEE Transactions on Microwave Theory and Techniques*, vol. 62, no. 10, pp. 2300-2307, 2014.
[26] F. Teberio, J.M. Percaz, I. Arregui, P. Martin-Iglesias, T. Lopetegi, M.A.G. Laso, and I. Arnedo "Rectangular waveguide filters with meandered topology," *IEEE Transactions on Microwave Theory and Techniques*, vol. 66, no. 8, pp. 3632-3643, 2018.
[27] Shang, M. Lancaster, and Y. Dong, "W-band waveguide filter based on large TM_{120} resonators to ease CNC milling," *Electronic Letters*, vol. 53, no. 7, pp. 488–490, 2017.
[28] D. Santiago, A. Tamayo-Domínguez, M.A.G. Laso, T. Lopetegi, J.M Férnandez-Gónzalez, R. Martínez, and I. Arregui, "Robust design of 3D-printed W-band bandpass filters using gap waveguide technology," *Journal of Infrared, Millimeter and Terahertz waves*, vol. 44, pp. 98-109, 2022.
[29] R. Sorrentino, P. Martin-Iglesias, O.A. Peverini, and T.M. Weller, "Additive manufacturing of radio-frequency components," *Proceedings of the IEEE*, vol. 105, no. 4, pp. 589-592, 2017.
[30] T. Chio, G. Huang, and S. Zhou, "Application of direct metal laser sintering to waveguide-based passive microwave components, antennas, and antenna arrays," *Proceedings of the IEEE*, vol. 105, no. 4, pp. 632-644, 2017.
[31] M. González-Calvo, J.R. Montejo-Garai, J.A. Ruiz-Cruz, and J.M. Rebollar, "Additive manufacturing of a high-performance Q -band circular TE_{01} mode flared-type transducer," *IEEE Microwave and Wireless Components Letters*, vol. 29, no. 9, pp. 577-579, 2019.
[32] M. Almeshehe, N. Murad, M. Rahim, O. Ayop, N. Samsuri, M.A. Aziz, and M. Osman, "Surface roughness impact on the performance of the 3D metal printed waveguide coupler at millimeter wave band,"*Engineering Science and Technology, an International Journal*, vol. 35, 2022.
[33] C.R. Garcia, R.C. Rumpf, H.H. Tsang, and J.H.Barton, "Effects of extreme surface roughness on 3D printed horn antenna," *Electronics letters*, vol. 49, no 12, p. 734-736, 2013.
[34] M. Ferrando-Rocher, J.I. Herranz-Herruzo, A. Valero-Nogueira, and B. Bernardo-Clemente, "Selective laser sintering manufacturing as a low cost alternative for flat-panel antennas in millimeter-wave bands," *IEEE Access*, vol. 9, pp. 45721-45729, 2021.
[35] E. Massoni, M. Guareschi, M. Bozzi, L. Perregrini, U.A. Tamburini, G. Alaimo, S. Marconi, F. Auricchio, and C. Tomassoni, "3D printing and metalization methodology for high dielectric resonator waveguide microwave filters," *IEEE MTT-S International Microwave Workshop Series on Advanced Materials and Processes for RF and THz Applications* (IMWS-AMP), pp. 1-3, 2017.
[36] C. Tomassoni, O.A. Peverini, G. Venanzoni, G. Addamo, F. Paonessa and G. Virone, "3D printing of microwave and millimeter-wave filters: additive manufacturing technologies applied in the development of high-performance filters with novel topologies," *IEEE Microwave Magazine*, vol. 21, no. 6, pp. 24-45, 2020.
[37] F. Romano, N. Delmonte, C. Tomassoni, L. Perregrini, and M. Bozzi, "3D-printed compact waveguide filters based on slanted ridge resonators," *IEEE/MTT-S International Microwave Symposium - IMS* 2022, pp. 96-99.
[38] R.G. Edwards, C.M. Norton, J.E. Campbell, and D. Schurig, "Effective conductivity of additive-manufactured metals for microwave feed components," *IEEE Access*, vol. 9, pp. 59979-59986, 2021.

David Santiago was born in Valencia, Spain, in 1994. He received the Telecommunication Engineering, and M.Sc. degrees from the Electrical, Electronic and Communications Engineering Department, Public University of Navarre (UPNA), Pamplona, in 2017, and 2019, respectively. He is currently pursuing the Ph.D. at the Public University of Navarre (UPNA).
His current research interests include the gap waveguide technology and coupled mode techniques applied to the synthesis of passive devices and structures employed in microwave, millimeter-wave, and terahertz (THz)-wave technologies.

Miguel A.G. Laso (Senior Member, IEEE) received the M.Sc. and Ph.D. degrees in telecommunications engineering from the Public University of Navarre (UPNA), Pamplona, Spain, in 1997 and 2002, respectively. From 1998 to 2001, he was a Doctoral Fellow Student with the Electrical and Electronic Engineering Department, UPNA, where he was an Assistant Professor from 2001 to 2006 and has been an Associate Professor (Professor Titular) since 2006, always involved in teaching and research duties related to optical communications and microwave engineering. From 2002 to 2003, he was also a Research Fellow with the Payload Systems Division, European Space Research and Technology Centre, European Space Agency (ESTEC-ESA), Noordwijk, The Netherlands. He is currently the Head of the Microwave Components Group (MCG), UPNA. He is the Co-Founder of TAFCO Metawireless S.L., a spin-off company of UPNA. He has authored or coauthored dozens of journal articles and contributed to major international conferences. He has also led projects with public and private funding within the MCG and UPNA. He holds several international patents. His current research interests include periodic structures, inverse scattering problems, synthesis techniques for filters and multiplexers in the microwave and millimeter-wave frequency ranges, and their applications in wireless and space communications. Dr. Laso has received several prizes, including the Spanish National Prize to the Best Doctoral Dissertation in telecommunications from the Spanish Telecommunications Engineers Association (COIT/AEIT) in 2002, the Junior Research Award of UPNA in 2003, and the 2005 Spanish National Prize for the Best Project in Innovation in Higher Education from the Spanish Ministry of Education and Science. He was an Associate Editor of IEEE TRANSACTIONS ON MICROWAVE THEORY AND TECHNIQUES from 2019 and 2022, and he is the current President of the URSI Spanish National Committee. He is also a member of several professional and scientific international associations, including the Optical Society of America (OSA), the International Society for Optics and Photonics (SPIE), and the American Society for Engineering Education (ASEE). He is also a TPRC Member of the MTT-S International Microwave Symposium (IMS) and a reviewer for several other international conferences and journals. He was the Co-Chair of the EuMC'18 (Madrid) and the Education Resources Development Subcommittee and is a member of MTT-5 Filters and the MTT-S Education Committee. He is also the Chair of the Working Group of Standards for Microwave Filter Definitions, IEEE Standards Committee.

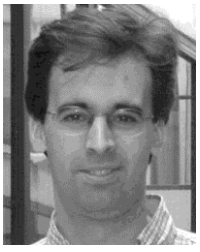

Txema Lopetegi (Member, IEEE) was born in Pamplona, Navarre, Spain, in 1973. He received the M.Sc. and Ph.D. degrees in telecommunication engineering from the Public University of Navarre (UPNA), Pamplona, in 1997 and 2002, respectively. Since 1997, he has been an Assistant Professor with the Electrical, Electronic and Communications Engineering Department, UPNA, where he has been an Associate Professor since 2006. From 2002 to 2003, he was a Research Fellow with the Payload Systems Division, European Space Research and Technology Centre (ESTEC), European Space Agency (ESA), Noordwijk, The Netherlands. He is the Co-Founder of TAFCO Metawireless S.L., a spin-off company of UPNA. His current research interests include

metamaterials and synthesized structures in microwave, millimeter-wave, and terahertz (THz) technologies, filters and passive components, coupled-mode theory and synthesis techniques using inverse scattering, and their applications in wireless and space communications. Dr. Lopetegi received a grant from the Spanish Ministry of Education in 1999 and 2000 to support the research in his doctoral thesis, several prizes including the Spanish National Prize to the Best Doctoral Dissertations in telecommunications in 2003 awarded by COIT/AEIT, and the Extraordinary Doctorate Prize of UPNA.

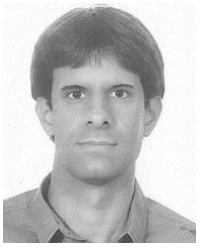

Ivan Arregui (Member, IEEE) received the Telecommunication Engineering, M.Sc., and Ph.D. degrees from the Public University of Navarre (UPNA), Pamplona, Spain, in 2005, 2008, and 2013, respectively. He is currently an Assistant Professor with the Electrical, Electronic and Communications Engineering Department, UPNA. He is the Co-Founder of TAFCO Metawireless S.L., a spin-off company of UPNA. His current research interests include periodic structure devices for microwave, millimeterwave, and terahertz frequency ranges, numerical techniques for the inversescattering synthesis, and the design of passive components for communications satellites. Dr. Arregui received a grant from the Spanish Ministry of Science and Innovation and several prizes, including the Junior Research Award of UPNA, the HISDESAT Prize from the Spanish Telecommunications Engineers Association (COIT/AEIT) for the Best Doctoral Dissertation in satellite services, and the Innovation Award from the Alberto Elzaburu Foundation.